Astron. manuscript no.
(will be inserted by hand later)

Your thesaurus codes are:
09 (09.09.1); (09.19.2); (13.25.4);

ASTRONOMY AND ASTROPHYSICS
October 3, 2000

# Detection of X-ray line emission from the shell of SNR B0540–69.3 with XMM-Newton RGS *

**K. J. van der Heyden[1], J. Cottam[2], F. Paerels[2], J. S. Kaastra[1], and G. Branduardi-Raymont[3]**

[1] SRON Laboratory for Space Research, Sorbonnelaan 2, 3584 CA Utrecht, the Netherlands
[2] Columbia Astrophysics Laboratory, Columbia University, 538 West 120th Street, New York, NY 10027, USA
[3] Mullard Space Science Laboratory, University College London, Holmbury St. Mary, Dorking, Surrey RH5 6NT, UK

Received ; accepted

**Abstract.** We present X-ray observations of PSR 0540–69.3 with the XMM-Newton observatory. The spectra obtained with the Reflection Grating Spectrometer reveal, for the first time, emission from ionized species of O, Ne and Fe originating from the SNR shell. Analysis of the emission line spectrum allows us to derive estimates of the temperature, ionization timescale, abundances, location, and velocity of the emitting gas.

**Key words:** ISM: individual: SNR 0540–69.3 – ISM: supernova – X-rays: ISM

## 1. Introduction

SNR 0540–69.3 is one of only a few Crab-like supernova remnants (SNRs) with a shell. SNR0540–69.3 harbors a pulsar, PSR B0540–69.3, discovered in the soft X-ray band by Seward, Harnden, & Helfand (1984). Like the Crab, it shows plerion emission from a synchrotron nebula powered by the embedded young pulsar (Chanan, Helfand & Reynolds 1984). From the period (50 ms) and spin down rate ($4.0 \times 10^{-13}$ss$^{-1}$) a a characteristic age of 1660 yr and rotational energy loss rate of $1.5 \times 10^{38}$ergs s$^{-1}$ have been derived (Seward, Harnden, & Helfand 1984).

Early optical observations (Mathewson et al. 1980) classified SNR 0540–69.3 as a young oxygen-rich SNR with an 8″ diameter shell, bright in [O III]. Mathewson et al. (1980) also found a diffuse patch of [O III] ~30″ to the west of the ring which indicated that the remnant was larger than 8″. A *ROSAT* High Resolution Imager observation by Seward & Harnden (1994) also revealed emission from well outside the central region, which they interpreted as from a patchy outer shell with a diameter of 55″. This shell contributes ~20% to the measured flux in the *ROSAT* 0.1–2 keV band. More recently Gotthelf & Wang (2000) presented a high resolution *Chandra* HRC observation of PSR B0540–69.3 which clearly shows emission from the outer shell.

*Send offprint requests to*: K. J. van der Heyden

* Based on observations obtained with XMM-Newton, an ESA science mission with instruments and contributions directly funded by ESA Member States and the USA (NASA).

In this letter, we report the results of observations of SNR 0540–69 acquired with the Reflection Grating Spectrometer on board the XMM-Newton Observatory (den Herder et al. 2001). These observations allow us for the first time to detect and identify emission lines from the remnant shell. Our spectral analysis allows us to derive values for the temperature, ionization timescale, abundances, location, and velocity of the emitting gas.

## 2. Observations & Data Reduction

PSR B0540 was observed repeatedly as part of the calibration of the Reflection Grating Spectrometer (RGS) during the Calibration/Performance Verification (Cal/PV) phase. For the purpose of this letter, we have analyzed the 126 ks data obtained on 2000 May 26, which is the longest observation with the lowest background. The observation was performed with the telescope rolled such that the RGS dispersion axis was aligned at 21.29°, clockwise on the sky, from celestial north. The data were initially processed with the XMM-Newton Science Analysis Software (SAS). The spectra were extracted by applying spatial filters to the CCD image while a CCD pulse-height filter was applied to select the $m = -1$ spectral order. The remnant is located on the edge of a broad region of diffuse emission (Wang & Helfand 1991) which complicates background determination. However, the image is small enough on the detector that spatial regions offset from the source position can be used for background subtraction. The background spectra were extracted by applying the same pulse height filters as used for the source, to spatial regions at either edge of the camera.

A response matrix appropriate to the spatial extent of the source was generated as follows. A spatial mask corresponding to the RGS aperture was imposed on the *Chandra* HRC image, and the intensity distribution was integrated over the RGS cross-dispersion direction. The resulting profile was convolved with the RGS point source response matrix, generated with the SAS task RGSRMFGEN. The spectral analysis was performed using the SRON SPEX (Kaastra et al. 1996) package, which contains the MEKAL code (Mewe et al. 1995) for modeling thermal emission.

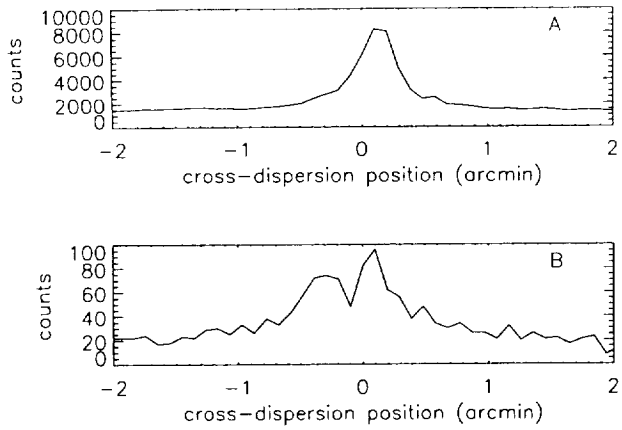


**Fig. 1.** Cross-dispersion profiles of SNR 0540–69 obtained by integrating along the dispersion axis for a: the entire spectrum and b: O VIII Ly$\alpha$ only.

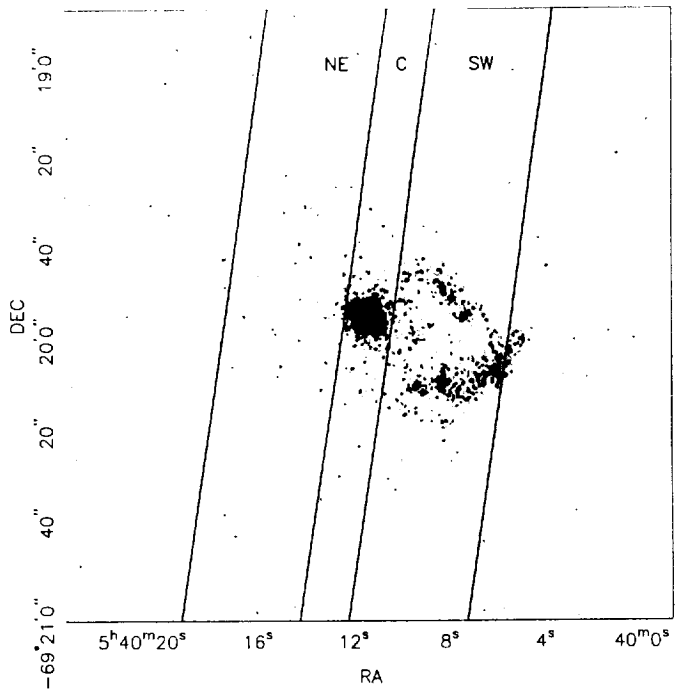


**Fig. 2.** X-ray image of SNR 0540–69.3 obtained by the *Chandra* HRC. The image contains the 50 ms pulsar PSR B0540–69.3, the plerion and the outer shell. The SW, C and NE regions used for spectral analysis are indicated. The disperion direction of the RGS is along the long dimension of the extraction regions.

## 3. Analysis and Results

### *3.1. Location of emitting region*

We initially extracted spectra with spatial filters 0.25′, 0.5′, 1′ and 1.5′ wide, each centered about the peak emission. The most interesting feature in the spectra is the presence of an O VIII Ly$\alpha$ emission line that becomes more prominent as the width of the spatial extraction region is increased. This is an indication that at least some of the O emission is from the SNR shell, and not the central region. To further constrain the spatial distribution of the emitting gas we created a cross-dispersion image profile of the O VIII Ly$\alpha$ line by integrating over the line in the dispersion direction. The cross-dispersion profile, plotted in Fig. 1, shows two peaks. Referring to the *Chandra* HRC image (Gotthelf & Wang 2000, reproduced here as Fig. 2), we conclude that we see O emission both from the central region of the remnant, centered on the pulsar, (the peak at offset zero in Fig. 1b), as well as from the partial shell to the west (the second peak $\approx$ 24 arcsec towards more negative offset in Fig. 2b).

The angular extent of this partial shell, $\Delta\phi \approx 30''$, corresponds to an effective wavelength width along the dispersion direction of $\approx$ 0.06 Å, comparable to the wavelength resolution of the spectrometer. This implies that we do not have the sensitivity to resolve variations in brightness along the shell.

### *3.2. Spectral analysis*

We divided the remnant into three regions, Northeast (NE), Central (C) and Southwest (SW), for the purpose of spectral analysis. For the NE and SW regions we use an extraction width of 0.5′centered at $\pm$0.375′ about the central compact region, while for the brighter C region we use a width of 0.25′. The spectra for these regions are displayed in Figs. 3 and 4. Each spectrum shows a strong power law continuum with superimposed line emission, most notably O VIII Ly$\alpha$. Emission line features are weakest in the spectrum extracted from the NE region, where we only detect O VIII Ly$\alpha$ and possibly weak O VII emission. The line emission is strongest in the SW spectrum where we easily identify emission lines of O VIII (Ly$\alpha$, Ly$\beta$), O VII ($n = 2 - 1$ triplet, He$\beta$), Fe XVII (15.01, 16.78, 17.05, 17.10 Å), Ne X (Ly$\alpha$), and Ne IX ($n = 2 - 1$ triplet). Due to galactic absorption, no features can be seen longward of $\sim$ 23 Å.

In the SW spectrum, O VIII Ly$\alpha$ has a significant offset of $\Delta\lambda = -0.17$ Å with respect to the laboratory wavelength. This offset must be largely due to a Doppler shift, and not to a positional offset between the nominal pointing direction (the pulsar position) and the emission centroid of the shell, because the equivalent wavelength extent of the shell is much smaller than the observed shift. This wavelength shift corresponds to a radial velocity of $v \sim -2700$ km s$^{-1}$.

We synthesized a spectral model comprising three components: a power law to represent the synchrotron emission from the plerion, a non-equilibrium ionization (NEI) model for the thermal line emission, and foreground absorption. The free parameters of the model are the photon index of the power law and its normalization, the electron temperature $T_e$, emission measure, abundances, ionization age $n_e t$ of the shocked gas, and the column density $N_{\rm H}$ of foreground absorbing gas. Here, $n_e$ is the electron density of the shell, and $t$ is the time since the hot gas was shocked. We adopt a distance of 51 kpc throughout.

We concentrated our quantitative analysis on the SW region since the spectrum from this region contains the strongest

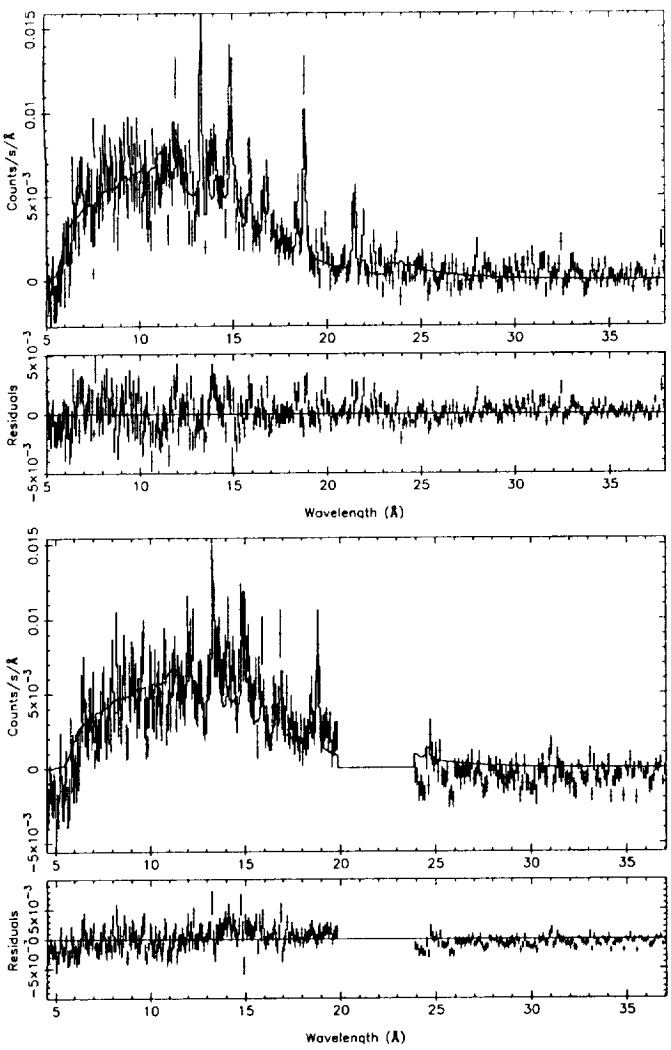


**Fig. 3.** RGS 1 & RGS 2 (upper and lower plots respectively) spectrum of the SW region. The solid line is a model fit to the data. The gap between 20 to 24 Å in the RGS 2 spectra is due to the failed CCD 4 on that instrument.The spectra exhibit a strong power law continuum due to synchrotron radiation from the plerion and thermal line emission from highly ionized atoms of O, Ne and Fe

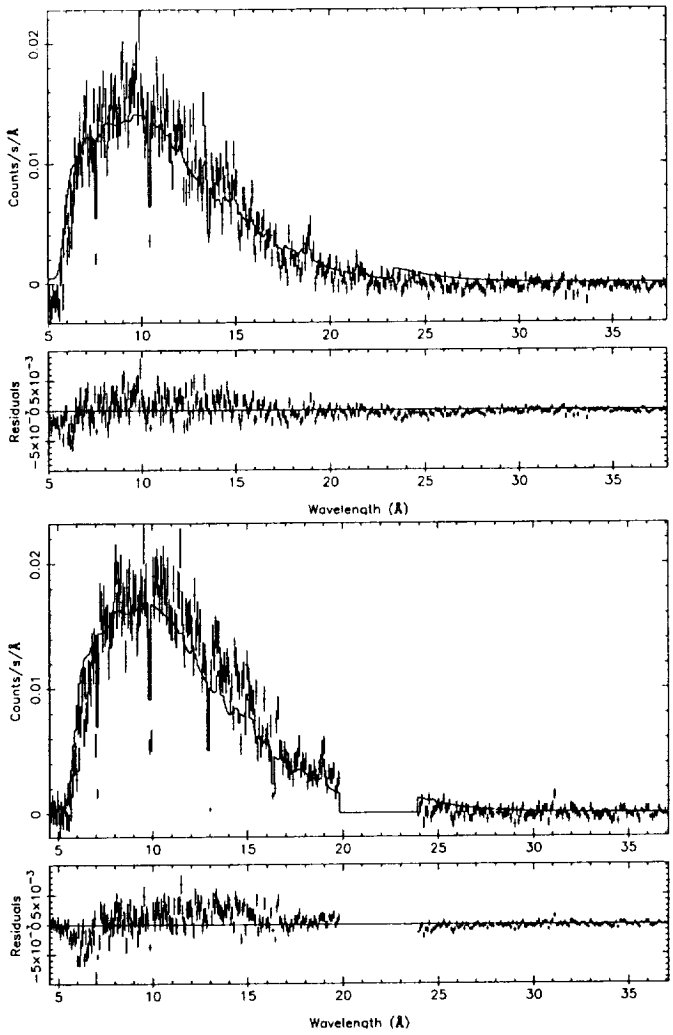


**Fig. 4.** Same as for Figure 3, but for the C region.

line emission features. Fixing the O abundance to a third solar (note that we have no independent way of constraining the absolute abundances, since the continuum emission is dominated by the plerionic emission), the abundances of Ne and Fe were allowed to vary with respect to O. An initial fit was made to the SW spectrum, using the O VIII Ly$\alpha$ and O VII-triplet only. The parameters obtained were subsequently used as starting parameters for fits to the entire spectrum. For the Ne/O and Fe/O abundance ratios, we obtain Ne/O $\sim$ 3.0 and Fe/O $\sim$ 2.1 relative to their solar values. The best fit model parameters are listed in Table 1. Fits were also made to the NE and C spectra. Since the line emission in these regions is extremely weak we fixed the NEI component parameters (i.e. electron temperature and ionization parameter) to the best fit parameters obtained from the SW region, while allowing the emission measure and photon indices of the power law component to vary. The best fit parameters are given in Table 1, and the spectra, together with the best fit models are shown in Figures 3, 4 and 5.

As can be seen from the Figures and the $\chi^2$ values in Table 1, the fits are not perfect. This is probably due to a combination of remaining small calibration uncertainties in the RGS effective area (up to $< 20$ %, shortward of 9 Å), and the simplicity of our spectral model, which does not allow for temperature and ionization inhomogeneities. In particular, there is a feature at $\approx$ 14 Å, which is not fit by our isothermal model. Candidate emission lines are $2p - 3d$ in Fe XVIII at 14.208 Å, or possibly $2s - 3p$ in Fe XXI at 14.008 Å, although the latter should be accompanied by strong emission at 12.29 Å in equilibrium. In any case, detectable amounts of higher charge states of Fe L would definitely indicate the presence of hotter plasma.

## 4. Discussion

First of all, a qualitative point. We detect faint, but significant O VIII emission from the direction of the plerion. At our spatial resolution, we cannot exclude the possibility that a significant

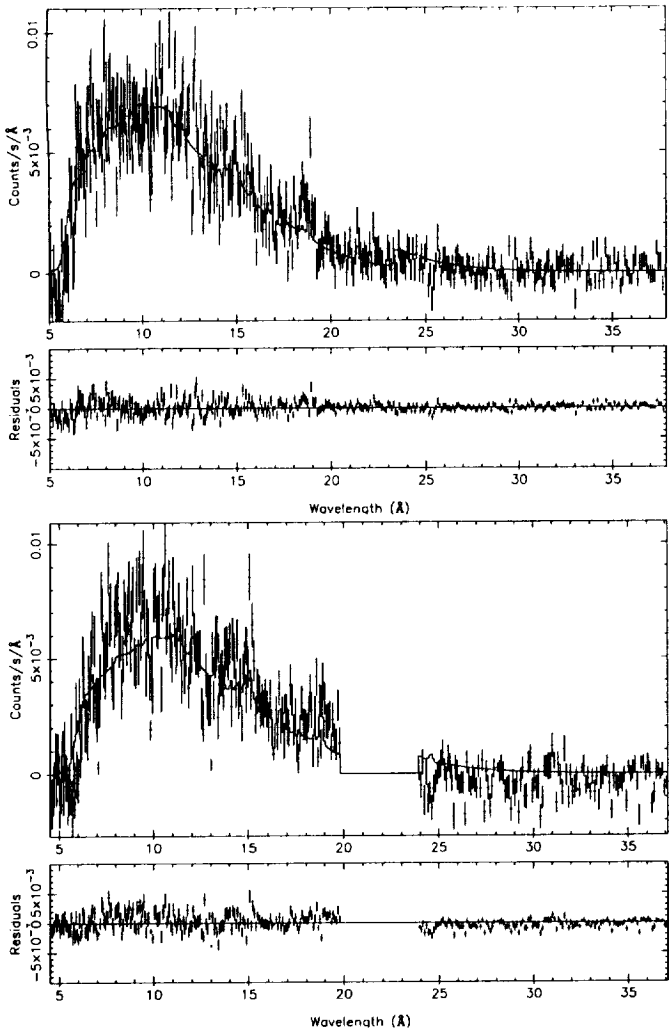


**Fig. 5.** Same as for Figure 3, but for the NE region.

**Table 1.** Fitting results for the SW, C and NE regions of SNR 0540–69.

| parameter | SW | C | NE |
|---|---|---|---|
| NEI: | | | |
| $n_e n_H V$ ($10^{58}$cm$^{-3}$) | 92±6.5 | 50±20 | 45±18 |
| $kT_e$ (keV) | 0.58±0.18 | | |
| $n_e t$ ($10^9$cm$^{-3}$s) | 25.22±5 | | |
| POW: | | | |
| photon index | 1.82±0.1 | 1.2±0.04 | 1.75±0.1 |
| ABS: | | | |
| $N_H$ ($10^{21}$cm$^2$) | 3.88±1 | | |
| $\chi^2$/d.o.f. | 2.04 | 2.8 | 2.9 |

component of this line emission is in fact from foreground remnant gas seen in projection. If confirmed at higher spatial resolution, this detection would be interesting, because Mathewson et al. (1980) detected intense optical [O III] emission from this same inner region, with a large velocity dispersion of $v \approx 3000$ km s$^{-1}$. There is evidently a wide range of ionization present in the plerion. Unfortunately, we do not have the sensitivity to try and localize the highly ionized oygen, and to constrain its kinematics for comparison with the [O III] image.

Next, we check for consistency of our measured parameter values. From the apparent expansion velocity of the shell, $v \sim 2700$ km s$^{-1}$, and its size, $\Delta\phi \approx 30''$, we deduce an expansion age of 2800 yr. Comparison with the pulsar spindown age then suggests that the shock has considerably slowed down, and that the shell has entered the adiabatic expansion phase. From the measured value of the ionization parameter, $n_e t \approx 2.5 \times 10^{10}$ cm$^{-3}$, and the pulsar spindown age, we estimate a charateristic density of $n_e \sim 0.5$ cm$^{-3}$ in the shell. The value of $n_e t$ itself indicates that the shocked gas has not yet reached ionization equilibrium. From the measured value of the emission measure, we can obtain an independent estimate for the density. Assuming half of a spherical shell of radius $30''$= 7.4 pc, and a relative thickness of one-tenth of the radius, we find $n_e \approx 10$ cm$^{-3}$, significantly above the value deduced from the ionization parameter. This discrepancy is most likely due to our crude estimate for the volume, and possibly by systematic uncertainties associated with the measurement of the emission measure (*i.e.* the fact that it is based on an isothermal model). Alternatively, we can take it as an indication that the shell is definitely inhomogeneous in density, temperature, and ionization.

A final consistency check can be based on calculating the initial supernova explosion energy from the Sedov solution for the shell parameters. We have, for the shell radius $R_s$, shock velocity $v_s$, and shock temperature $T_s$ ( e.g. Lozinskaya 1992)

$$R_s = 12.9 t_4^{2/5} (\frac{E_0}{n_0})^{1/5} \mathrm{pc} \quad (1)$$

$$v_s = 505 t_4^{-3/5} (\frac{E_0}{n_0})^{1/5} \mathrm{kms}^{-1} \quad (2)$$

$$T_s = 3 \times 10^6 t_4^{-6/5} (\frac{E_0}{n_0})^{2/5} \mathrm{K}, \quad (3)$$

with $n_0 = n_e/4$ the density of the ambient medium, $E_0$ the explosion energy in units $7.5 \times 10^{50}$ erg, and $t_4$ the time since the explosion, in units $10^4$ yr. Assuming $R_s = 7.4$ pc, $v_s = 2700$ km s$^{-1}$, $kT_s = 0.58$ keV, $t_4 = 0.166$, and $n_e = 0.5$ cm$^{-3}$, we find explosion energies of $2.1 \times 10^{50}$, $1.9 \times 10^{51}$, and $2.8 \times 10^{48}$ erg, derived from the estimates for the shell size, expansion velocity, and temperature, respectively. This range is too large for consistency, and the last estimate, based on the shock temperature, appears very low. This we take as another positive indication that the shell is not homogeneous. Note that Seward and Harnden (1994) were essentially forced to assume $kT_e \sim 5$ keV in their analysis of the *ROSAT* HRI image, in order to obtain consistency with the value for the explosion energy estimated from the shell radius.

## 5. Conclusions

We have detected resolved X-ray thermal line emission from the supernova remnant shell around PSR B0540–69.3. We find

a spectroscopic expansion velocity of $v_s \sim -2700$ km s$^{-1}$. We estimate values for the average shock temperature and ionization age, and find that the shell appears to be underionized. From a comparison of the geometric expansion age, and the pulsar spindown age we conclude that the shell has entered the adiabatic expansion phase. However, from apparent inconsistencies for the initial explosion energies as estimated from the Sedov expressions for the shell parameters, we conclude that the shell is inhomogeneous, which is not surprising, given its appearance in the high resolution *Chandra* HRC image.

## 6. Acknowledgements

We thank Eric Gotthelf for supplying us with his *Chandra* HRC image. The Laboratory for Space Research Utrecht is supported financially by NWO, the Netherlands Organization for Scientific Research. The Columbia group is supported by the U.S. National Aeronautics and Space Administration. The Mullard Space Science Laboratory acknowledges financial support form the UK Particle Physics and Astronomy Research Council.

## References

Chanan, G.A., Helfand, D.J., & Reynolds, S., 1984, ApJ, 287, L23
den Herder, J. W. et al. 2001, A&A, this issue.
Gotthelf, E.V., & Wang, Q.D., 2000, ApJ, 532, L117
Kaastra, J.S., Mewe, R., Nieuwenhuijzen, H.1996, in UV and X-ray Spectroscopy of Astrophysical and Laboratory Plasmas, p. 411, eds. K. Yamashita and T. Watanabe, Tokyo, Univ. Ac. Press
Lozinskaya, T. A. 1992, 'Supernovae and Stellar Wind in the Interstellar Medium', (New York: American Institute of Physics), p.206
Mathewson, D.S., Dopita, M.A., Tuohy, I.R., & Ford, V.L., 1980, ApJ, 242, L73
Mewe, R., Kaastra, J.S., Liedahl, D.A., 1995, Legacy 6, 16
Seward F.D., Harnden Jr F.R., & Helfand D.J., 1984, ApJ, 287, L19
Seward F.D, & Harnden Jr F.R., 1994, ApJ, 421, 581
Wang Q.D., & Helfand D.J., 1991, ApJ, 379, 327